CrystEngComm

Accepted Manuscript

ROYAL SOCIETY OF CHEMISTRY

www.rsc.org/crystengcomm

Continuous cocrystallisation of Carbamazepine and trans-Cinnamic acid via melt extrusion processing

Hiren G. Moradiya, Muhammad T. Islam, Sheelagh Halsey[2], Mohammed Maniruzzaman, Babur Chowdry[1], Martin J. Snowden[1], D. Douroumis*

[1]University of Greenwich, Faculty of Engineering and Science, Chatham Maritime, Chatham, ME4 4TB, Kent, UK.

[2]Thermo Fisher Scientific, Molecular Spectroscopy and Material Characterization, Hemel Hempstead, HP2 7GE, UK

Table of Contents

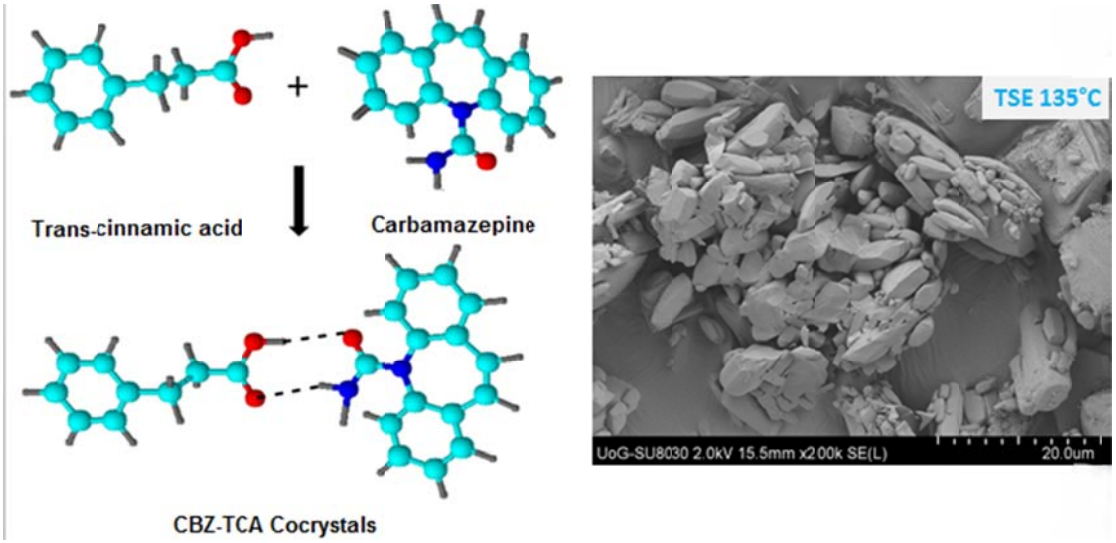

High quality of carbamazepine – trans cinnamic acid (BBZ-TCA) cocrystals were produced through continuous Hot Melt Extrusion processing. Single and twin – screw extrusion was employed to optimize the obtained cocrystals in comparison to a prototype produced by solvent crystallization. In – line NIR studies revealed that CBZ –TCA corystals were formed gradually along the mixing zones of the extruder. The manufactured cocrystals showed improved dissolution rates.

Abstract

A solvent free process for the formation of Carbamazepine (CBZ) - trans Cinnamic acid (TCA) cocrystals, at stoichiometric ratios, was developed using continuous Hot Melt Extrusion processing. Physicochemical characterization of the CBZ-TCA extrudates included scanning electron microscopy (SEM) differential scanning calorimetry (DSC), X-ray powder diffraction (XRPD) and hot stage microscopy to evaluate the shape, morphology, purity and crystallinity of the freshly made cocrystals. The obtained cocrystals were of high quality compared to the prototype produced by a solvent crystallization technique. Furthermore, an in-line NIR probe was implemented to investigate the gradual formation of cocrystals during extrusion processing. The quality of the CBZ-TCA cocrystals was found to depend on the processing parameters such as temperature and the screw type. The extruded cocrystals showed faster dissolution rates compared to bulk CBZ and the prototype cocrystals.

Introduction

The development of novel drug formulations and processing technologies has been traditionally explored by of pharmaceutical industry and still remains among the main focuses. This has a profound importance for the development of poorly water-soluble active pharmaceutical ingredients (APIs) as approximately 40% of drugs in the pipeline have very low water solubility. The lack of efficient formulation and processing technologies can reduce the commercial potential of such drugs.

Up to date, cocrystals are an emerging formulation approach in pharmaceutical drug development aiming to improve solubility, dissolution, bioavailability and stability [1- 5] of various water-poorly soluble drugs. In addition to the physicochemical improvements of the drug molecules, cocrystals can highly be patentable as a completely new drug entity. Cocrystals have been viewed as a supramolecular perspective, which involves understanding of intermolecular interactions between the API and the conformer candidates [6, 7]. Cocrystals held by low energy non covalent interactions such as hydrogen bonds, van der Wall forces or π-bonds without changing the chemical and physiological action of drug compound. Cocrystals are formed as homogenous phases between two or more molecular components in the crystalline lattice where usually consists of a drug substance and a co-crystal coformer [8]. Moreover, according to Food and Drug Administration (FDA) guidelines pharmaceutical, "cocrystals are crystalline materials composed of two or more molecules in the same crystalline lattice". [9]

The solvent crystallization and mechanical grinding, are the two most common processes that are regularly used to produce pharmaceutical cocrystals[10, 11] but in reality both of these techniques, are time consuming and difficult to scale-up. Excessive use of solvent can be harmful and costly as well and a small residue of the solvent or impurities [12] can be toxic which can again raise regulatory issues. The solubility of the active compounds in organic solvents can lead to undesired solvates formation [13]. Some other techniques such as spray drying [14], ultra-sonication [15], supercritical fluid techniques [16] hydration [17] ink – jet printing [18] and microfluidic antisolvent [19] crystallization have also been used for the development and engineering of various pharmaceutical cocrystals.

HME has been introduced in the pharmaceutical industry and it is now widely utilised as a highly versatile and robust process. HME has found several applications in formulation development including solubility and bioavailability enhancement or taste masking of bitter

APIs through the manufacturing of amorphous solid dispersion Recently, HME gained significant interest in pharmaceutical research for the manufacturing and engineering of cocrystals [20, 21]. HME is considered a continuous process with excellent scalability, high throughput efficacy intense mixing capacity and low residence time compared to traditional technologies. The absence of any organic solvents or water during processing makes HME an environmental friendly technology.

Cinnamic acid is an excellent coformer for the formation of cocrystals formation which mainly interacts through hydrogen bonding (in some limited extent via p-stacking [22] or van der Waals forces) with its hydroxyl group. Carbamazepine (CBZ) has been reported as a model drug for the formation of cocrystals due to the presence of the amide functional group, which react with a range of cocrystal formers. Recently published research showed that cocrystals of carbamazepine-cinnamic acid can effectively prevent the conversion of CBZ to its dihydrate form which could be attributed to the relatively lower solubility of the coformer explained stronger stability of cocrystals in aqueous media[23]. Highly water soluble coformers are thermodynamically unstable and transform to CBZ dehydrate form when placed in aqueous mediums.

The ability to monitor and in some extent to potentially control the quality attributes of cocrystals in real-time would be an effective tool aligning with the current regulatory initiatives towards continuous monitoring. In the recent years, process understanding is strongly supported by the Food and Drug Administration (FDA) agency though the implementation of quality by design (QbD) and process analytical technology (PAT) tools [24]. As a result, the scope of the real time data interpretation, continuous quality monitoring and control has led PAT to enjoy a renaissance in continuous manufacturing and product development. Up to date various PAT tools have been employed in the area of crystallization such as UV–visible, NIR and Raman spectroscopic techniques [25].

Here, we report a solvent free novel cocrystallisation process of carbamazepine and trans-cinnamic acid by using both single screw (SSE) and twin screw extrusion (TSE) processing. In addition we investigate the ability of near infrared spectroscopy (NIR) to monitor the formation of cocrystals produced in a continuous mode during twin-screw extrusion.

Materials and methods

Materials

Pure carbamazepine form III (CBZ, purity ≥ 98%) and trans-cinnamic acid (TCA, purity ≥ 99%) were purchased from Sigma Aldrich (Gillingham, UK) and used as received. All solvent used for HPLC analysis were analytical grade.

Solvent crystallization of CBZ-TCA cocrystals (SCP)

Cocrystals of CBZ -TCA blends were produced by solvent crystallization and used as reference (prototype) [26]. Briefly, CBZ and TCA at 1:1 molecular ratio were dissolved in ethyl acetate followed by heating for 5 minutes at 75°C. The prepared solution was left to evaporate for 72 hours and subsequently the dried cocrystals were collected for further evaluation.

Hot-melt extrusion processing

The extrusion was performed by using both a single screw, (RCP 0625, Randcastle, USA) and Eurolab 16 twin-screw extruders (Thermofisher, Germany) without the die. Equimolar amounts of CBZ and TCA were weighed and blended thoroughly in a T2F Turbula mixer (Willy A. Bachofen AG, Switzerland) for 10 minutes. Preliminary studies (results not shown) revealed that the optimal processing temperature should not exceed 135°C for both SSE and TSE processes (30-50-110-125-135-135-135-130-110^{o}C). The screw speed was kept at 10 rpm.

Scanning electron Microscopy (SEM)

The morphology of all extruded samples including the bulk CBZ and TCA was examined by SEM (Hitachi SU8030, Japan). Samples were placed on double sided carbon tape sticks on an aluminium stub and coated with thin layer of chromium in argon an atmosphere at room temperature. The accelerating voltage of the electron beam was 2KV to get the SEM images.

Differential Scanning Calorimetry (DSC) analysis

DSC was used to evaluate the solid state of the samples including bulk substances, physical blend and the extruded formulations collected from different barrel zones. The samples weighed in crimped aluminium pan and heated from 25°C to 200°C (Mettler Toledo 823e, Greifensee, Switzerland) at a heating rate of 10^{o}C/min. Pure nitrogen gas was used as a purge

gas and was supplied at 20ml/min. The Star evaluation software was used for post experimental analysis.

Hot Stage Microscopy (HSM)

The hot stage microscopy analysis was conducted with Mettler Toledo FP82HT (Leicester-UK) hot stage instrument supplied with microscope (Leica microsystems, China). Samples were scattered on a glass slide and heated from ambient temperature to 200°C at a heating rate of 10°C/min. Changes in morphology behaviour in all samples were collected as a video recording by using PixeLINK PL-A662 camera (PixeLINK, Ontario, US).

X-ray powder diffraction (XRPD) analysis

XRPD was used to determine the solid state of bulk materials, physical mixtures and extrudates using a Bruker D8 Advance (Germany) in theta-theta mode. For the study purposes a Cu anode at 40kV and 40Ma, parallel beam Goebel mirror, 0.2 mm exit slit, LynxEye Position Sensitive Detector with 3° opening (LynxIris at 6.5 mm) and sample rotation at 15 rpm were used. Each sample was scanned from 2 to 40° 2Θ with a step size of 0.02° 2Θ and a counting time of 0.3 seconds per step; 176 channels active on the PSD making a total counting time of 52.8 seconds per step.

***In vitro* dissolution study**

Dissolution studies were carried out in USP II paddle apparatus (Varian 705, US). Equal amount to 200 mg of bulk CBZ, CBZ-TCA extruded powders and prototype were placed into 900 ml of 0.1 M (pH 1.2) HCl in each dissolution vessel (n=3). The temperature of the media was maintained at 37^{o}C with a paddle rotation at 100 rpm. About 2-3ml of samples were withdrawn at 15, 30, 60 and 120 min intervals and filtered with a 200µm filter prior to HPLC analysis.

Drug content analysis

HPLC analysis carried out with an AGILENT 1200 series HPLC (USA) instrument equipped with auto sampler. Mobile phase was prepared with 60:40 ratios of Na mono-phosphate buffer (pH 7.3) and acetonitrile. Zorbex Eclipse C8 (4.6×150 mm×5 µm) column from Agilent, USA was used with 1 ml/minute flow rate at 254 nm wavelength. The calibration curve was constructed by varying the standard solutions with 10-50 µg/ml concentration.

Physical stability study

Bulk CBZ and extruded TSE cocrystals were placed in open glass vials and exposed to pre equilibrated accelerated condition (40^{o}C and 75 % RH ± 5 %) created with supersaturated solution of sodium chloride (Sigma Aldrich, Germany) and at 40°C ± 2°C for six months.

In-line near infra-red (NIR) spectroscopy monitoring

Diffuse reflectance near infrared (NIR) spectroscopy was continuously performed in-line and non-invasively during hot-melt extrusion using an Antaris MX Fourier Transform NIR spectrometer (Thermo Scientific, UK). A fibre optic NIR probe was fitted in three different zones of extruder barrel for in-line monitoring. Spectra were collected in the 10000-4000 cm^{-1} region with a resolution of 16 cm^{-1}. Each spectrum taken was an average of 32 individual scans which took around 16 s to complete. In addition to real-time monitoring, the extruded cocrystal spectra were measured off-line. Off-line NIR spectra were also collected for the bulk carbamazepine, bulk saccharin and the physical mixture of both. Data analysis was performed by using the RESULT software (version 3.0, Thermo Scientific, UK)

Results and discussion

HME processing

Cocrystals were collected in the powder form as the die, which is usually placed at the end of extruder to shape the extrudates, was removed. Temperature profiles were found to play a key role in SSE extrusion and influence the cocrystal properties. Extrusion trials carried out with SSE revealed that the temperature profile set at a maximum of 135ºC formed extruded cocrystals of better quality compared to those at 125°C. Attempts to process the blends at lower temperatures (110^{o}C) showed that extrusion could not take place, while at higher temperatures (150^{o}C) the formation of cocrystals was not successful (supplementary DSC graph). As the spiral screw design [27] of SSE was unable to provide better material mixing**,** further optimization of extruded cocrystals carried out with TSE equipment by optimizing the temperature. During TSE processing, screw configuration was adjusted to achieve excellent mixing by assembling the kneading elements in three separate “mixing zones” as shown if Fig. 1. Extruded samples were collected from each zone to investigate the effect of the

kneading elements and provide a better understanding of cocrystallization process (discussed in following sections).

SEM analysis revealed differences in the shape and size between extruded cocrystals and bulk components which is a strong indication of molecular interactions among the bulk compounds. Bulk CBZ seemed micronized, flaky or thin plate liked materials while TCA has disc shaped crystals (Fig. 2). All HME treated cocrystals were found clumped with undistributed geometry, as they did not undergo further particle size reduction. The TSE cocrystals were more clustered compare to SSE where several micro-crystals packed together to form larger particles. This could be possibly attributed to the effect of the mixing zones of the twin–screw extruder. The prototype cocrystals were found polyhedral prismatic with smaller particle size distribution compared to the extrudates.

Thermal analysis

DSC was employed to evaluate the solid state of the pure components as well as the extruded cocrystals. Analysis of thermal transition of bulk CBZ indicated the existence of polymorphic form III as the melting peak appeared at 175.14°C (ΔH 15.40 J/g) followed by a subsequent phase transformation leading to the melt at 192.39°C (ΔH 99.93 J/g) (Fig. 3). The thermogram of bulk TCA showed an endothermic thermal transition due to its melting at 134.55°C (ΔH 145.47 J/g) (Fig. 3). The physical blend of CBZ-TCA at 1:1 molar ratio showed one minor endotherm at 93.92°C (ΔH 4.90 J/g) and two other main endotherms at 121.81°C (ΔH 25.49 J/g) and 141.69°C (ΔH 99.40 J/g) respectively as shown in Fig. 4 The first transition at 120°C corresponds to the shifted peak of TCA while the second endothermic peak refers to the eutectic of the cocrystal made of the melting of CBZ in TCA[8].

Cocrystals processed by SSE at 125°C and 135°C showed a single endothermic blunt peak at 137.72°C (ΔH 58.79 J/g) and 138.46°C (ΔH 61.67 J/g), respectively. The endothermic peak suggests single structured system while the blunt shape of the peak points out the presence of unreacted amorphous or crystalline portion of material left in SSE extruded products. Despite the fact that SSE produced high torque, sufficient to form cocrystals, the lack of dispersive mixing resulted in low quality (reduced crystallinity) cocrystals.

A single and sharp endothermic peak was observed in the thermogram (Fig. 3) of the extruded cocrystals processed with $TSE_{135°C}$ which is quite similar to that of the prototype cocrystals obtained by the solvent crystallization process (SCP). The thermogram of the

CBZ-TCA cocrystal processed via TSE showed a sharp melting transition at 141.20^{o}C (ΔH 92.62J/g) while the prototype at 143.08 (ΔH 114.46 J/g). The TSE cocrystals were of high quality (>99%).and similar to those produced with the prototype (data not shown).

Furthermore, Fig. 4 shows the DSC thermographs of the materials collected at three different mixing zones during TSE processing. By comparing the thermograms of the sample collected from Zone A and the PM it can be seen that they are almost identical (except the peak at 93.92°C) suggesting no major crystal transformation of the processed blends.

In contrast, the thermal transitions of the processed materials collected from Zone B presented a sharp melting peak at 141.84°C which corresponds to the final melting point of the stable cocrystals but with some evidence of unreacted material at 121.41°C. The complete formation of CBZ-TCA cocrystals occurred in Zone 3 where the absence of the small endothermic peak is evident.

HSM studies were conducted to visually determine the thermal transitions and the extent of drug melting within the TCA used at different stages of heating. DSC results were in good agreement with HSM findings. Cocrystals processed with SSE_{125oC} melt at 138°C in HSM but still some untreated materials were observed at even above150°C. However, vapour produced from the sample made the image bit darker which was eventually been cleared at around 185°C. It was assumed that the evaporation is related to the melting of the remaining CBZ in the cocrystal lattice. Interestingly, this was not the case for the extruded cocrystals processed both by SSE and TSE at 135°C. As shown in Fig. 5 extruded cocrystals at 135^{o}C presented different melting behaviour depending on the extrusion processing whereas for SSE and TSE melting occurred at 138.46°C and 141.20°C respectively.

XRPD analysis

X-ray diffractograms of physical blends, pure components, prototype and processed cocrystals at different extrusion zones are illustrated in Fig 6, 7. In Fig.6, it can be seen that cocrystals processed with SSE at 125^{o}C and 135^{o}C showed lower intensity peaks indicating the presence of unreacted materials. In contrast, cocrystals processed via SSE at 135^{o}C presented higher intensity diffraction peaks.

In Fig. 7 it can clearly be seen that the formation of cocrystals started in the 2nd mixing zone and new intensity peaks appeared at 5.78 and 7.57^{o} 2θ values. The same peaks with very low

intensity were observed in Zone 1 including intensity peaks that correspond to bulk CBZ and TCA. It is obvious that both components started to interact at molecular level in Zone 1 while in the 2nd mixing zone, the peaks at 15.30 °, 15.87 °, 24.94°2θ are eliminated. Finally, the cocrystals formation was completed in Zone 3 with the appearance of diffraction peaks at 5.83°, 7.57°, 9.91°, 16.66°, 21.82°, and 27.33°2θ values which are identical to those of the prototype. Apparently, the screw configuration in Zone 2 played a crucial role for the initiation of the cocrystallization process temperature while the placement of the mixing elements at 60 and 90° angles in Zone 3 resulted in cocrystals with improved crystallinity.

NIR spectroscopy

Off-line NIR spectra of CBZ, TCA and the physical mixture (PM) were measured to identify the characteristic peaks attributed to the cocrystals. From Fig. 8 it can be easily seen that the NIR spectra of CBZ and TCA present characteristic peaks at different wavelengths. The spectrum of the PM is represented by the combined spectra of the bulk materials. The second derivative NIR spectra of the PM, CBZ and the co-former in the 4600-5300 cm^{-1} region are shown in Fig. 9. The spectrum of TCA is almost flat where those of CBZ and the PM are identical and only the peak intensities are different.

Fig. 10 depicts the second derivative spectra of the PM and the extruded cocrystals that show significant differences due to the peak shifts. The peak at 5044 cm^{-1} was due to the N-H stretching. This was observed shifting to 4988 cm^{-1} as the H-bond formed between CBZ and TCA. The new peak became more intense as cocrystallization increased. The peak shifting at lower wavenumbers could be attributed to the formation of hydrogen bonding as a result of the formation of cocrystals between CBZ and TCA.

As the CBZ-TCA blends are transferred within the conveying and mixing zones, the formation of cocrystals is expected to gradually take place along the barrel. In order to study further the cocrystal formation, the NIR probe was carefully placed in the three mixing zones and the in-line scans were collected. Fig. 11 shows the second derivative spectra of the three different mixing zones, the final extruded cocrystals in comparison to the PM. Formation of CBZ-TCA cocrystals starts in the second mixing zone and a peak appears at 4988 cm^{-1}. The spectra obtained for zones B and C shows an increase in the new peak as the extrudate moves towards the end of the extruder. The off-line scan of the final extruded CBZ-TCA cocrystals present the highest intensity suggesting the completion of the process.

These findings suggest that cocrystals were formed gradually due to the increasing mixing capacity across the three mixing zones. The effect of the dispersive and distributive mixing has been previously observed in a recent study where high quality cocrystals prepared with a TSE in comparison to a SSE [28]. In addition, Kelly et al. (2012)[29] showed that high intensity mixing (dispersive) has a significant effect on the quality of the formed cocrystals. The influence of the dispersive mixing is well known in the extrusion of drug-polymer blends where is has been found to increase the drug dissolution of water insoluble drugs[30]. We assumed that better quality cocrystals are formed due to the dispersive mixing of the TSE resulting the breakage of the solid domains in fine morphologies (SEM analysis). The contribution of distributive mixing should not be excluded but it requires additional investigation. A schematic representation of the H-bonding between the CBZ and TCA molecules is depicted in Fig. 12.

In vitro dissolution studies

In vitro dissolution studies were conducted to assess the performance of produced cocrystals compared to the bulk CBZ. As shown in Fig. 13 a slow dissolution rate of 49% after 2hr was observed for bulk CBZ. In contrary, SSE processed cocrystals at 125 and 135^{o}C showed significant dissolution rate increase with more than 50% after one hour. However, the dissolution of the SSE_{125oC} cocrystals was limited at 60% after 120min while for the SSE_{135oC} reached a maximum of 76%. Nevertheless, the TSE_{135oC} cocrystals presented the higher rates with 50% CBZ dissolution within the first 10min and 70% after 1hr. Eventually, 90% CBZ release was observed after 120min, compared to 81% of the prototype. The SSE cocrystals showed fast dissolution rates especially for the first 60 min in comparison to the prototype but slower compared to the TSE_{135oC}. Interestingly the higher amorphous content of CBZ in the SSE_{125oC} cocrystals did not facilitate faster dissolution rates. As a result the faster dissolution rates are related to the higher purity of the developed cocrystals. In addition, as shown in Fig. 14 the influence of the particle size distribution was excluded as bulk CBZ presented smaller particle size while the extruded samples and the prototype consisted of larger particles.

Physical stability

Stability studies of the produced HME cocrystals (SSE and TSE) at accelerated conditions (40 °C and 75% RH) showed excellent stability without any changes in the crystallinity after 6 months. Further XRPD analysis showed identical intensity peaks as a result of the crystal

integrity. In addition, no visual alterations in morphology or colour of cocrystals were observed.

Conclusions

In this study, cocrystals of CBZ-TCA were continuously manufactured by using SSE or TSE processing. The barrel temperature and the screw type were found to affect the quality of the produced cocrystals. The dissolution rates of the cocrystals were found to increase with an ascending order of bulk CBZ< SSE< SCP < TSE. Twin screw extrusion processing produced cocrystals with faster dissolution rates compared to single screw but also to the solvent crystallization approach. In line NIR analysis showed a gradual development of cocrystals across the three extrusion zones through the formation of hydrogen bonding. Cocrystals were stable over six months under accelerated conditions. In conclusion HME is a robust continuous process for the manufacturing of high quality, stable drug cocrystals facilitating drug – conformer interactions.

References

1) M. B. Hickey, M. L. Peterson, L.A. Scoppettuolo , S. L. Morrisette, A. Vetter A, H. Guzman , J. F. Remenar, Z. Zhang , M.D. Tawa, S.Haley, M.J. Zaworotko and O. Almarsson, *Eur. J. Pharm. Biopharm.,* 2007, **67**, 112-119.
2) D. McNamara, S. Childs, J. Giordano ,A. Iarriccio ,J. Cassidy, M. Shet, R. Mannion, E. O'Donnell and A. Park, *Pharm. Res.,* 2006, **23**, 1888-1897.
3) A. V. Trask, W. D. S. Motherwell and W. Jones, *Int. J. Pharm.*, 2006, **320**, 114-123.
4) J. W. Steed, *Trends Pharmacol. Sci.*, 2013, **34**, 185-193.
5) N. Blagden, M. de Matas, P.T. Gavan and P. York, *Adv. Drug Delivery Rev.*, 2007, **59**, 617–630.
6) G. R. Desiraju, *Angew. Chem., Int. Ed. Engl.,* 1995, **34**, 2311-2327.
7) C. B. Aakeroy, N. R. Champness and C. Janiak, *Crystengcomm,* 2010, **12**, 22-43.
8) E. Lu, N. Rodriguez-Hornedo and R. Suryanarayanan, *CrystEngComm,* 2008, **10**, 665-668.
9) Guidance for Industry: Regulatory Classification of Pharmaceutical Cocrystals http://www.fda.gov/downloads/Drugs/Guidances/UCM281764.pdf
10) A. Yadav, A. Shete, A. Dabke, P. Kulkarni and S. Sakhare, *Indian J. Pharm. Sci.*2009, **71**, 359–370.

11) M. B. Hickey, Ö. Almarsson and M. L. Peterson, *CrystEngComm*, 2012, **14**, 2349-2349.

12) K. H. Y. Hsi, K. Chadwick, A. Fried, M. Kenny and A. S. Myerson, *CrystEngComm*, 2012, **14**, 2386-2388.

13) Al. Alhalaweh and S. P. Velaga, *Cryst. Growth Des*, 2010, **10**, 3302-3305.

14) AV. Trask, W. Jones, *Org. Solid-State React.,* 2005, **254**, 41-70.

15) S. Aher, R. Dhumal, K. Mahadik, A. Paradkar and P. York, *Eur. J. Pharm. Sci.,* 2010, **41**, 597-602.

16) L. Padrela , M. A. Rodrigues ,S. P. Velaga, H. A. Matos and E.G. de Azevedo, *Eur. J. Pharm. Sci.*, 2009, **38**, 9-17.

17) C.B. Aakeröy, S. Forbes and J. Desper, *CrystEngComm*, 2012, **14**, 2435 - 2443.

18) A.B.M. Buanz, R. Telford, I.J. Scowen, S. Gaisford, *CrystEngComm*, 2013,**15**, 1031-1035

19) M. R. Thorson, S. Goyal, Y. Gong, G. G. Zhang, and P. J. Kenis, *CrystEngComm*, 2012, **14**, 2404-2412.

20) R. S. Dhumal, A. L. Kelly, P. York, P. D. Coates and A. Paradkar, *Pharm. Res.,* 2010, **27**, 2725-2733..

21) B. S. Sekhon, (2009), *Ars Pharm.*, **50**, 99-117.

22) D. Daurio, C. Medina, R. Saw, K. Nagapudi and F. Alvarez-Núñez, *Pharmaceutics,* 2011, **3**, 582-600.

23) A. Shayanfar, K. Asadpour-Zeynali and A. Jouyban, *J. Mol. Liq.,* 2013, **187**, 171-176.

24) CDER, 2004 Office of Pharmaceutical Sciences, Process and Analytical Technologies Initiative, http://www.fda.gov/cder/OPS/PAT.htm.

25) L. Saerens, L. Dierickx, B. Lenain, C. Vervaet, J. P. Remon and T. De Beer, *European Eur. J. Pharm. Biopharm.,* 2011, **77**, 158-163.

26) J. A. McMahon, Master of Science Thesis, University of South Florida, 2006.

27) K. Luker, *Hot-melt Extrusion:Pharmaceutical Applications*, ed. D. Douroumis, John Wiley & sons ltd, UK, 1st edn., 2012, ch. 1, pp. 1-21.

28) H. Moradiya, M. T. Islam, G.R. Woollam, I. J. Slipper, S. Halsey,M.J. Snowden and D. Douroumis, *Crystal Growth & Design*, 2013, **14**, 189-198.

29) A.L. Kelly, T. Gough T, R.S. Dhumal, S.A. Halsey and A. Paradkar, *Int. J. Pharm.*, 2012, **426**, 15-20.

30) H. Liu, P. Wang, X. Zhang, F. Shen and C. G. Gogos, *International journal of pharmaceutics*, 2010, **383**, 161-169.

Figure Caption List

Figure 1 Schematic diagram of screw in TSE indicates collection zones

Figure 2 SEM micrographs of bulk CBZ, bulk TCA, cocrystals manufactured with SSE_{125^oC}, SSE_{135^oC} and TSE_{135^oC}

Figure 3 DSC thermograms of bulk CBZ, bulk TCA, cocrystals processed with SSE_{125^oC}, SSE_{135^oC}, TSE_{135^oC} and the physical mixture.

Figure 4 DSC thermograms of samples were collected from different zones in TSE with prototype prepared from solvent method.

Figure 5 HSM images of cocrystals manufactured with SSE, TSE and solvent crystallization (prototype)

Figure 6 X-ray diffractograms of SSE_{125^oC}, SSE_{135^oC} and TSE_{135^oC} cocrystals.

Figure 7 X-ray diffractograms of the physical mixture and samples from TSE barrel zones (A, B and C)

Figure 8 NIR spectra of bulk CBZ, bulk TCA, and CBZ-TCA physical mixture

Figure 9 Second derivatives NIR spectra of CBZ (bulk), TCA, and CBZ-TCA physical mixture at the region of 4600-5300 cm^{-1}

Figure -10 Second derivative spectra of CBZ-TCA (PM) and the extruded cocrystals in the region between 4600-5300 cm^{-1}

Figure -11 Second derivative of in-line NIR spectra in the mixing zones (A, B, C), the TSE extruded cocrystals and the physical mixture.

Figure 12 3D-molecular modelling of the developed CBZ-TCA cocrystals illustrating the H-bonding between the functional groups

Figure 13 Dissolution profiles of bulk CBZ, prototype (solvent method) and extruded cocrystals (pH 1.2 HCl, n=3)

Figure 14 Particle size distribution of bulk CBZ, extrudates batches (SSE_{125^oC}, SSE_{135^oC}, TSE_{135^oC}) and prototype cocrystals

Schematic diagram of screw in TSE indicates collection zones
9x0mm (300 x 300 DPI)

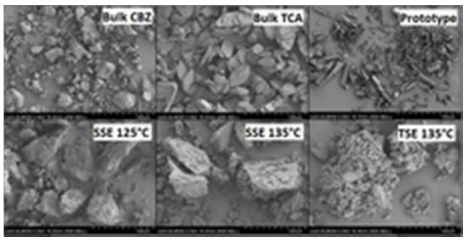

SEM micrographs of bulk CBZ, bulk TCA, cocrystals manufactured with SSE125ºC, SSE135ºC and TSE135ºC
19x9mm (300 x 300 DPI)

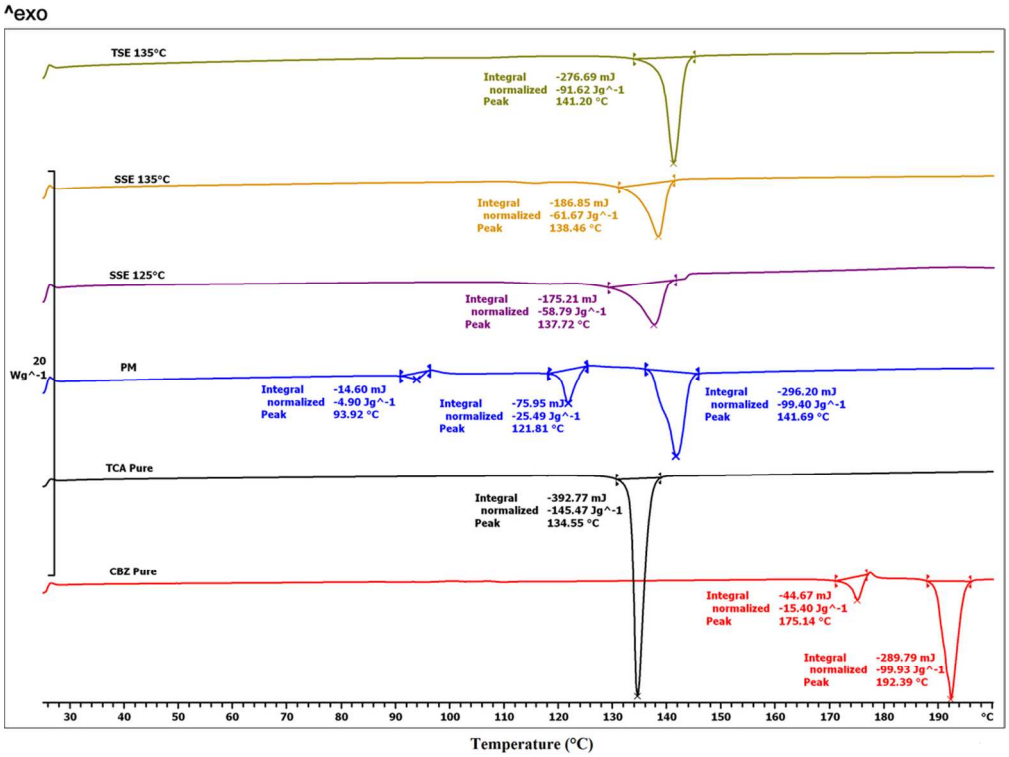

DSC thermograms of bulk CBZ, bulk TCA, cocrystals processed with SSE125ºC, SSE135ºC, TSE135ºC and the physical mixture.
96x73mm (300 x 300 DPI)

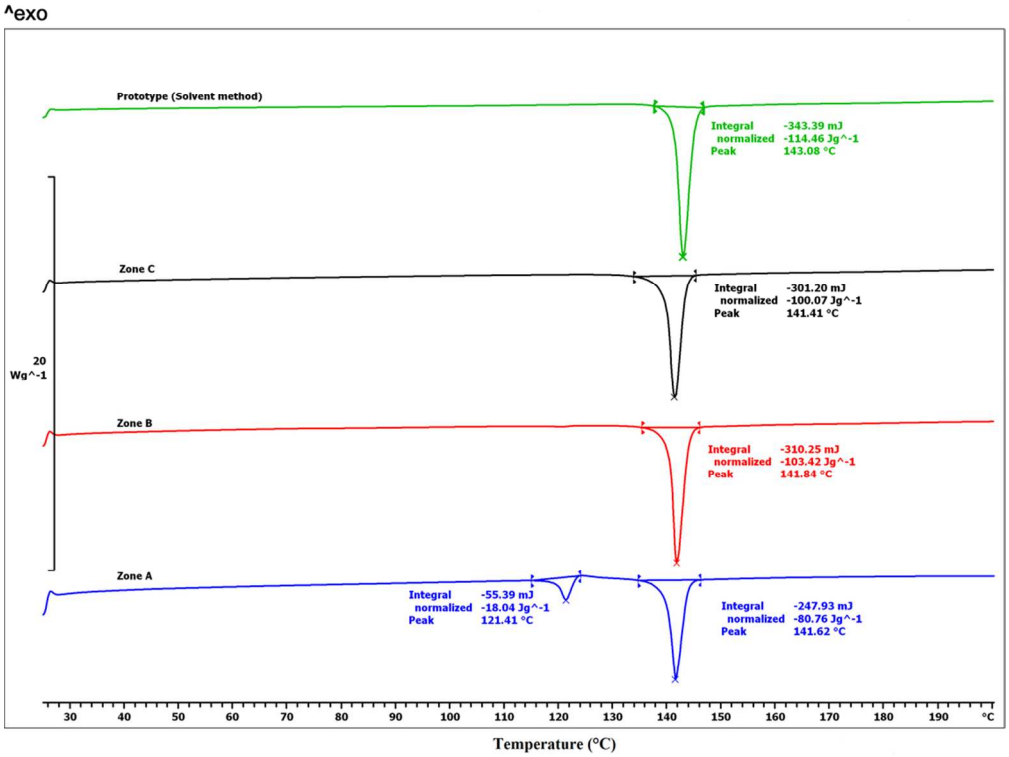

DSC thermograms of samples were collected from different zones in TSE with prototype prepared from solvent method.
96x73mm (300 x 300 DPI)

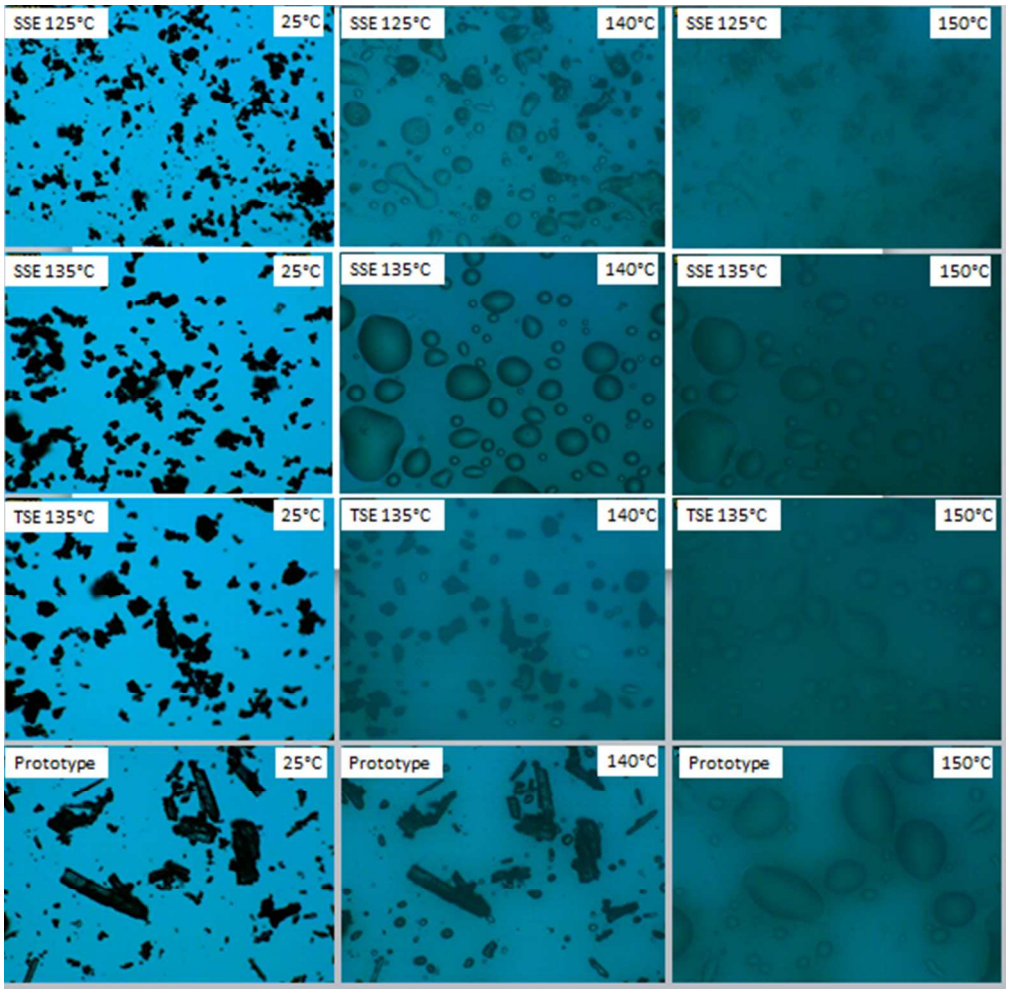

HSM images of cocrystals manufactured with SSE, TSE and solvent crystallization (prototype)
47x46mm (300 x 300 DPI)

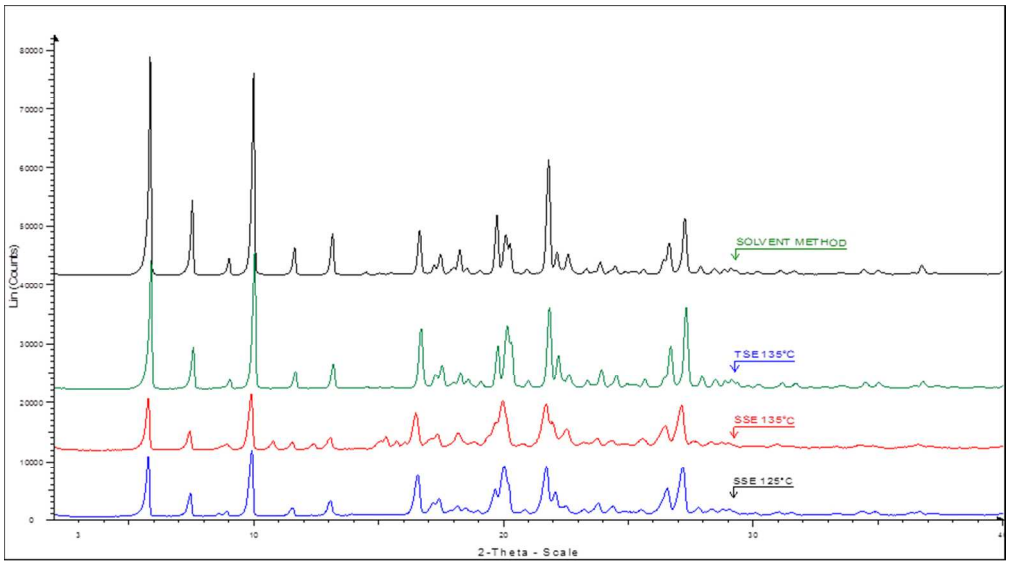

X-ray diffractograms of SSE125ºC, SSE135ºC and TSE135ºC cocrystals.
249x138mm (96 x 96 DPI)

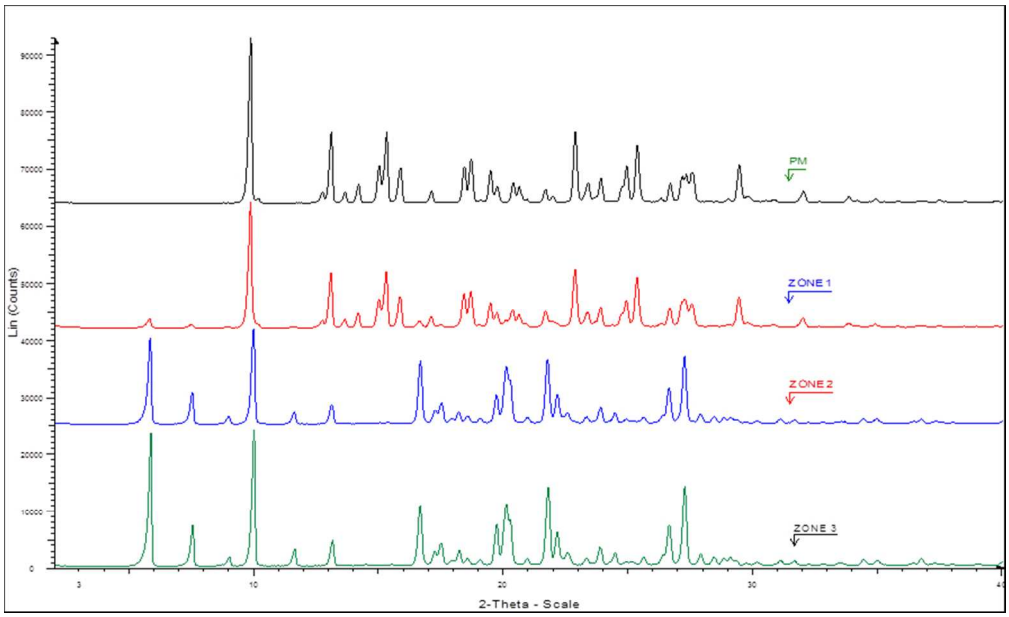

X-ray diffractograms of the physical mixture and samples from TSE barrel zones (A, B and C)
235x142mm (96 x 96 DPI)

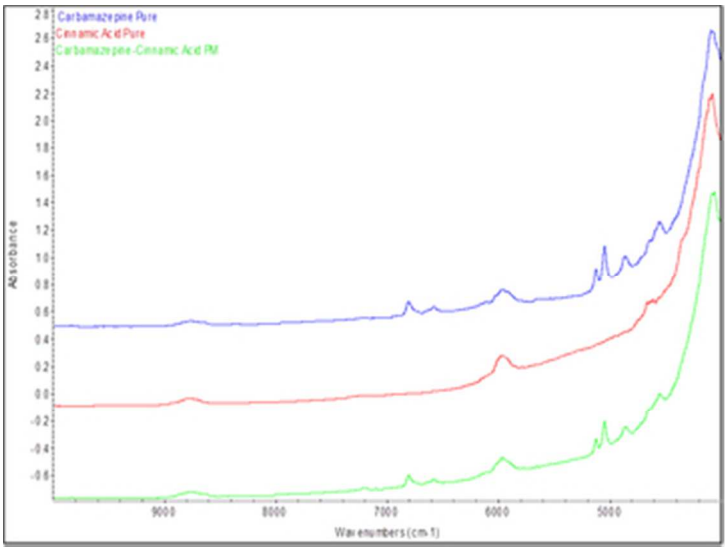

NIR spectra of bulk CBZ, bulk TCA, and CBZ-TCA physical mixture
30x22mm (300 x 300 DPI)

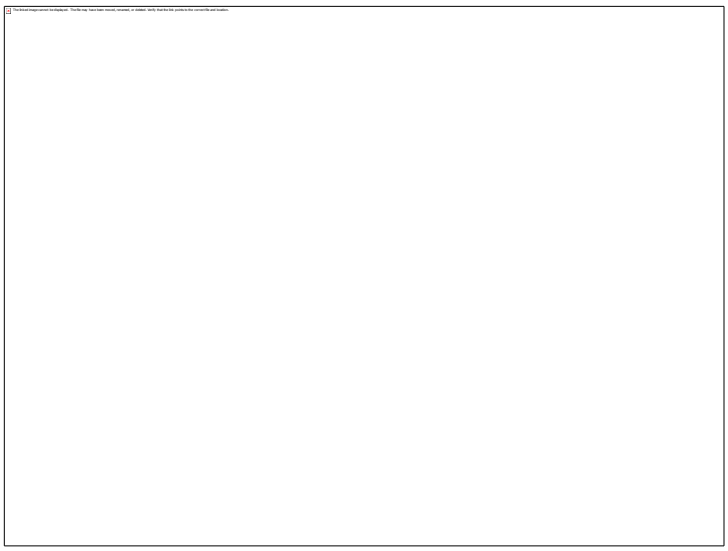

Second derivatives NIR spectra of CBZ (bulk), TCA, and CBZ-TCA physical mixture at the region of 4600-5300 cm-1
30x22mm (300 x 300 DPI)

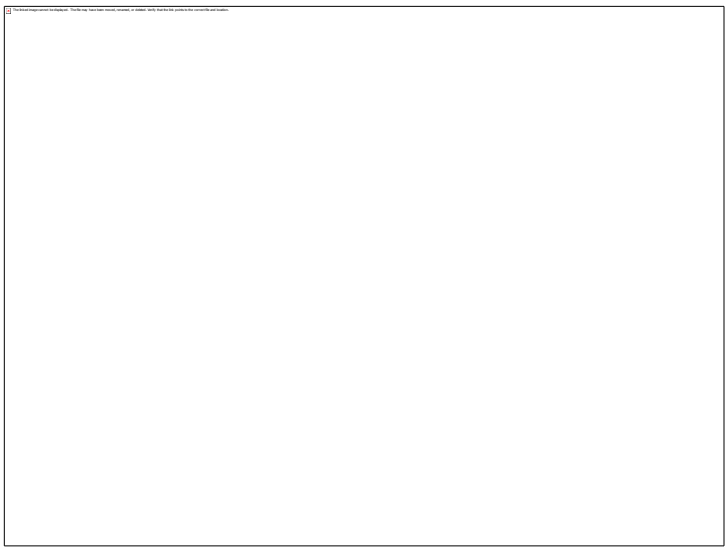

Second derivative spectra of CBZ-TCA (PM) and the extruded cocrystals in the region between 4600-5300 cm-1
30x22mm (300 x 300 DPI)

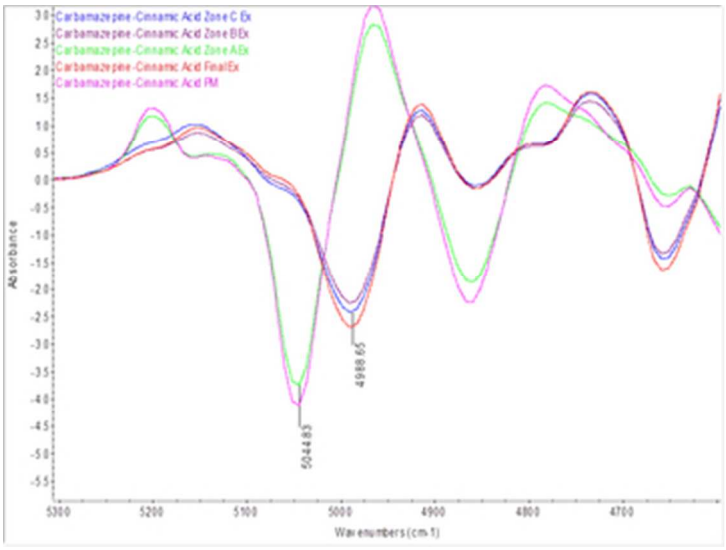

Second derivative of in-line NIR spectra in the mixing zones (A, B, C), the TSE extruded cocrystals and the physical mixture.
30x22mm (300 x 300 DPI)

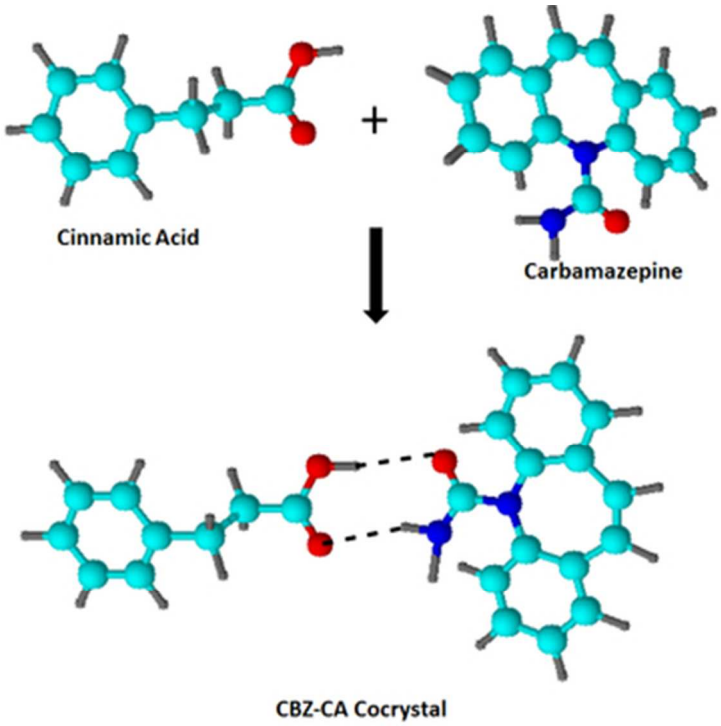

3D-molecular modelling of the developed CBZ-TCA cocrystals illustrating the H-bonding between the functional groups
30x30mm (300 x 300 DPI)

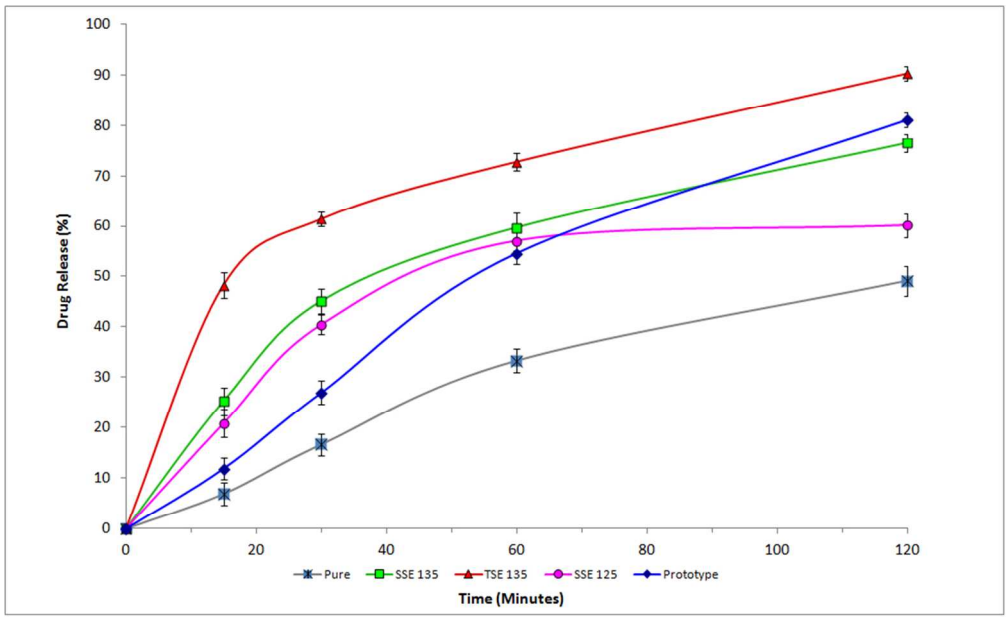

Dissolution profiles of bulk CBZ, prototype (solvent method) and extruded cocrystals (pH 1.2 HCl, n=3)

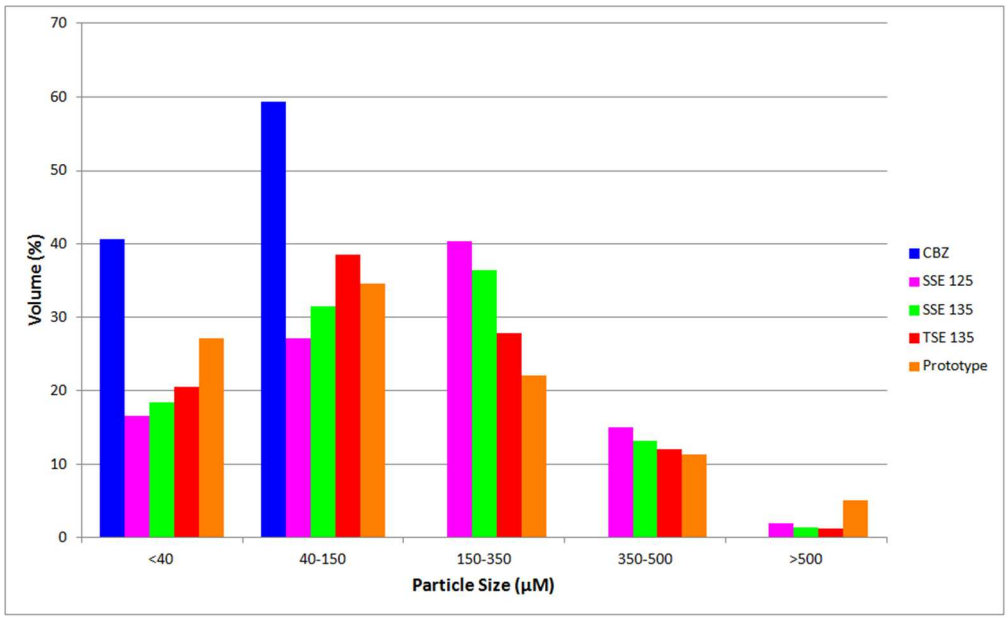

Particle size distribution of bulk CBZ, extrudates batches (SSE125ºC, SSE135ºC, TSE135ºC) and prototype cocrystals